Molecular Therapy
Nucleic Acids
Original Article

N4-acetylcytidine acetylation of neurexin 2 in the spinal dorsal horn regulates hypersensitivity in a rat model of cancer-induced bone pain

Longsheng Xu,[1] Shang Zheng,[1] Liping Chen,[1] Lei Yang,[1] Shuyao Zhang,[1] Beibei Liu,[1] Kangli Shen,[1] Qinli Feng,[1] Qinghe Zhou,[1] and Ming Yao[1]

[1]Department of Anesthesia and Pain Medicine, Affiliated Hospital of Jiaxing University, Jiaxing 314000, China

Cancer-induced bone pain (CIBP) significantly impacts the quality of life and survival of patients with advanced cancer. Despite the established role of neurexins in synaptic structure and function, their involvement in sensory processing during injury has not been extensively studied. In this study using a rat model of CIBP, we observed increased neurexin 2 expression in spinal cord neurons. Knockdown of neurexin 2 in the spinal cord reversed CIBP-related behaviors, sensitization of spinal c-Fos neurons, and pain-related negative emotional behaviors. Additionally, increased acetylation of neurexin 2 mRNA was identified in the spinal dorsal horn of CIBP rats. Decreasing the expression of N-acetyltransferase 10 (NAT10) reduced neurexin 2 mRNA acetylation and neurexin 2 expression. In PC12 cells, we confirmed that neurexin 2 mRNA acetylation enhanced its stability, and neurexin 2 expression was regulated by NAT10. Finally, we discovered that the NAT10/ac4C-neurexin 2 axis modulated neuronal synaptogenesis. This study demonstrated that the NAT10/ac4C-mediated posttranscriptional modulation of neurexin 2 expression led to the remodeling of spinal synapses and the development of conscious hypersensitivity in CIBP rats. Therefore, targeting the epigenetic modification of neurexin 2 mRNA ac4C may offer a new therapeutic approach for the treatment of nociceptive hypersensitivity in CIBP.

INTRODUCTION

Cancer-induced bone pain (CIBP) is a symptom of bone metastasis in advanced cancer (e.g., breast, prostate, or lung cancer) patients, with a high prevalence rate between 75% and 90%.[1,2] However, current clinical treatments for CIBP are limited, and the available analgesic drugs are commonly associated with significant toxic side effects, such as somnolence, constipation, and respiratory depression.[3] Recently, the role of epigenetics in chronic pain development has emerged as a prominent research area.[4,5] This field holds promise for unraveling the molecular etiology of CIBP and providing a theoretical foundation for developing novel and effective therapeutic interventions for CIBP.

Previous studies have focused on common RNA modifications, such as m6A, m5C, m1A, and m7G modifications.[6,7] N4-acetylcytosine RNA acetylation (ac4C) is a conserved chemical modification that occurs at the N4 position of acetylcytosine, catalyzed by an RNA ac4C-modifying enzyme.[8] Currently, ac4C modification represents a novel class of RNA modifications with potential significance in the field of epitranscriptomics, akin to m6A modification.[9] In protein covalent modifications, acetylation/deacetylation has been established as the second most important factor in post-transcriptional regulation and is closely associated with pain.[10,11] However, there is limited research on the modulation of chronic pain through RNA acetylation. In this study, we focused on mRNA ac4C from an epigenetic perspective to elucidate the molecular basis underlying neural pathway maladaptation in the bone cancer microenvironment and its role in CIBP development and maintenance.

The neurexins family comprises highly polymorphic cell surface proteins that are specifically expressed in mammalian neurons.[12] The extensive polymorphism and synaptic localization of neurexins suggest their involvement in cell surface receptor function, cell recognition, and adhesion.[13] Potential effects of neurexins include (1) interaction with neuroligins (neuronal cell adhesion molecules on the postsynaptic membrane) to facilitate functional synapse formation[14,15]; (2) acting as presynaptic receptors with high affinity for α-latrotoxin in the presence of Ca^{2+} to induce synaptic vesicle cytosolization and stimulate neurotransmitter release[16,17]; (3) serving as endogenous ligands that tightly bind to neurexins in the brain, potentially regulating intracellular signaling in specific neuronal subpopulations[18]; (4) non-Ca^{2+}-dependent tight binding of Ca^{2+} receptor-synaptotagmins to neurexins, potentially playing a vital role in synaptic vesicle docking and targeting in nerve terminals[19,20]; and (5) binding of the LNS structural domains of neurexins to dystroglycan for synaptogenesis or neuron-astrocyte interactions.[21] Collectively, the neurexin family regulates both synaptic structure and

Received 8 February 2024; accepted 21 April 2024;
https://doi.org/10.1016/j.omtn.2024.102200.

Correspondence: Qinghe Zhou, Department of Anesthesia and Pain Medicine, Affiliated Hospital of Jiaxing University, Jiaxing 314000, China.
E-mail: zqh10980@zjxu.edu.cn
Correspondence: Ming Yao, Department of Anesthesia and Pain Medicine, Affiliated Hospital of Jiaxing University, Jiaxing 314000, China.
E-mail: jxyaoming@zjxu.edu.cn

function. While the precise function of neurexin 2 remains unclear, we hypothesized that neurexin 2 plays a crucial role in synaptic plasticity based on currently available information.

A CIBP model was created by injecting 10 μL Walker-256 breast cancer cell suspension into the bone marrow cavity of the left tibia of Sprague-Dawley rats.[22–24] Our previous research identified the widespread distribution of ac4C in the spinal dorsal horn (SDH) L4–L6 transcriptome of rats by ac4C-specific RNA immunoprecipitation assay (acRIP-seq). The differential genes with ac4C mRNA modification and mRNA expression in CIBP rats revealed a significant correlation, suggesting that ac4C is involved in the development of CIBP.[25] Further analysis of the ACHPA (4-amino-5-cyclohexyl-3-hydroxy pentanoic acid)-containing renin inhibitory peptide sequencing data identified neurexin 2 as one of the highly correlated differential genes. The study investigated the expression changes of neurexin 2 mRNA ac4C in the spinal cord of rats with CIBP and their correlation with pain thresholds through the use of acRIP-qPCR, molecular biology techniques, and pain behavior tests. Additionally, small interfering RNA (siRNA), RIP-qPCR, and pain behavior tests were employed to study the mutual regulation of N-acetyltransferase 10 (NAT10), neurexin 2 mRNA ac4C, and neurexin 2, as well as their roles in pain sensitization in rats with CIBP. Last, electron microscopy and related molecular biology techniques were utilized to examine the impact of the NAT10-ac4C-neurexin 2 axis on spinal cord synaptic plasticity in rats with CIBP.

The results of the study demonstrated that bone cancer increased the acetylation of the neurexin 2 mRNA and increased its half-life through NAT10. The upregulated expression of neurexin 2 initiated spinal cord synaptic plasticity and contributed to the development of nociceptive hypersensitivity in rats with CIBP. Overall, this study investigated the mechanisms underlying CIBP, and the findings of this study may potentially contribute to the development of novel strategies and targets for preventing and treating CIBP.

RESULTS

Expression and cellular localization of neurexin 2 in the SDH tissue of rats with CIBP

CIBP development is closely associated with synaptic plasticity in the central nervous system.[26] The neurexins family plays a crucial role in synaptic assembly and functional regulation.[27] Neurexin 2 may have a substantial impact on the development of CIBP.

To investigate the potential role of neurexin 2 in CIBP, a rat model of CIBP was established. Mechanical pain abnormalities were assessed in rats from the CIBP model group and the sham group at various time points, including preoperative and postoperative days 3, 6, 9, 12, 15, and 18. The results demonstrated that CIBP rats exhibited heightened sensitivity to mechanical stimuli from day 6 to day 18, as evidenced by a significant decrease in the foot reduction threshold (Figure 1A). Gait analysis further confirmed these findings, revealing a lower maximum pressure intensity, mean pressure intensity, and plantar area of the paw in CIBP rats after postoperative day 9 (Figures 1B and 1C), thus validating the successful establishment of the CIBP model.

Subsequently, SDH tissues were collected from rats in the sham and CIBP groups, and the expression of neurexin 2 was analyzed using qPCR, western blotting, and immunofluorescence techniques. The results demonstrated that neurexin 2 mRNA and protein expressions in the SDH of CIBP rats were significantly increased on days 9 and 15 (Figures 1D–1F). Immunofluorescence analysis further revealed upregulated neurexin 2 expression in the ipsilateral spinal cord of CIBP rats on postoperative day 9 (Figure 1G). Co-localization assays with markers for neurons (NeuN), astrocytes (GFAP), and microglia (Iba1) demonstrated that neurexin 2 primarily co-localized with the neuronal marker NeuN in the SDH tissues (Figure 1H). Furthermore, a negative correlation was observed between pain threshold and neurexin 2 expression in CIBP rats, indicating that higher neurexin 2 expression was associated with lower pain thresholds (Figure 1I).

These findings suggested that neurexin 2 may play a critical role in CIBP development. Further investigations are warranted to elucidate the specific mechanisms underlying the contribution of neurexin 2 to CIBP.

Downregulation of neurexin 2 reverses pain behavior and spinal neuron sensitization in rats with CIBP

To investigate the involvement of neurexin 2 in the development of bone cancer-induced nociceptive sensitization, siRNA oligonucleotide sequences targeting neurexin 2 were transfected into the SDH tissues of rats.

In the evaluation of mechanical nociceptive hypersensitivity in rats with CIBP, rats in the CIBP, CIBP+MC-siRNA, and CIBP+neurexin2-siRNA groups exhibited mechanical nociceptive hypersensitivity as compared with the sham group on postoperative day 7 (Figure 2A). Intrathecal administration of neurexin 2 siRNA on days 6, 8, and 10 resulted in a significant increase in the mechanical withdrawal threshold of rats in the CIBP+neurexin 2-siRNA group on days 9, 11, and 13, respectively (Figure 2A), indicating that inhibition of neurexin 2 expression reversed the mechanical nociceptive sensitization in rats with CIBP. The results of CatWalk gait analysis also confirmed that with intrathecal administration of siRNA on postoperative days 6 and 8, the maximum contact area, mean intensity, and maximum contact intensity were elevated in the ipsilateral (left)/contralateral (right) hind paw percentage on day 9 in the CIBP rats in the neurexin 2-siRNA group as compared with the rats in the MC-siRNA group (Figures 2B and 2C). Detection of pain-related negative emotional behavioral changes on postoperative day 9 revealed that CIBP rats in the CIBP+neurexin 2-siRNA group exhibited increased time and number of explorations in the bright field of the bright-dark shuttle, as well as increased time and number of explorations into the open arm in the elevated cross maze. Additionally, the number of buried beads was significantly decreased in the CIBP+neurexin 2-siRNA

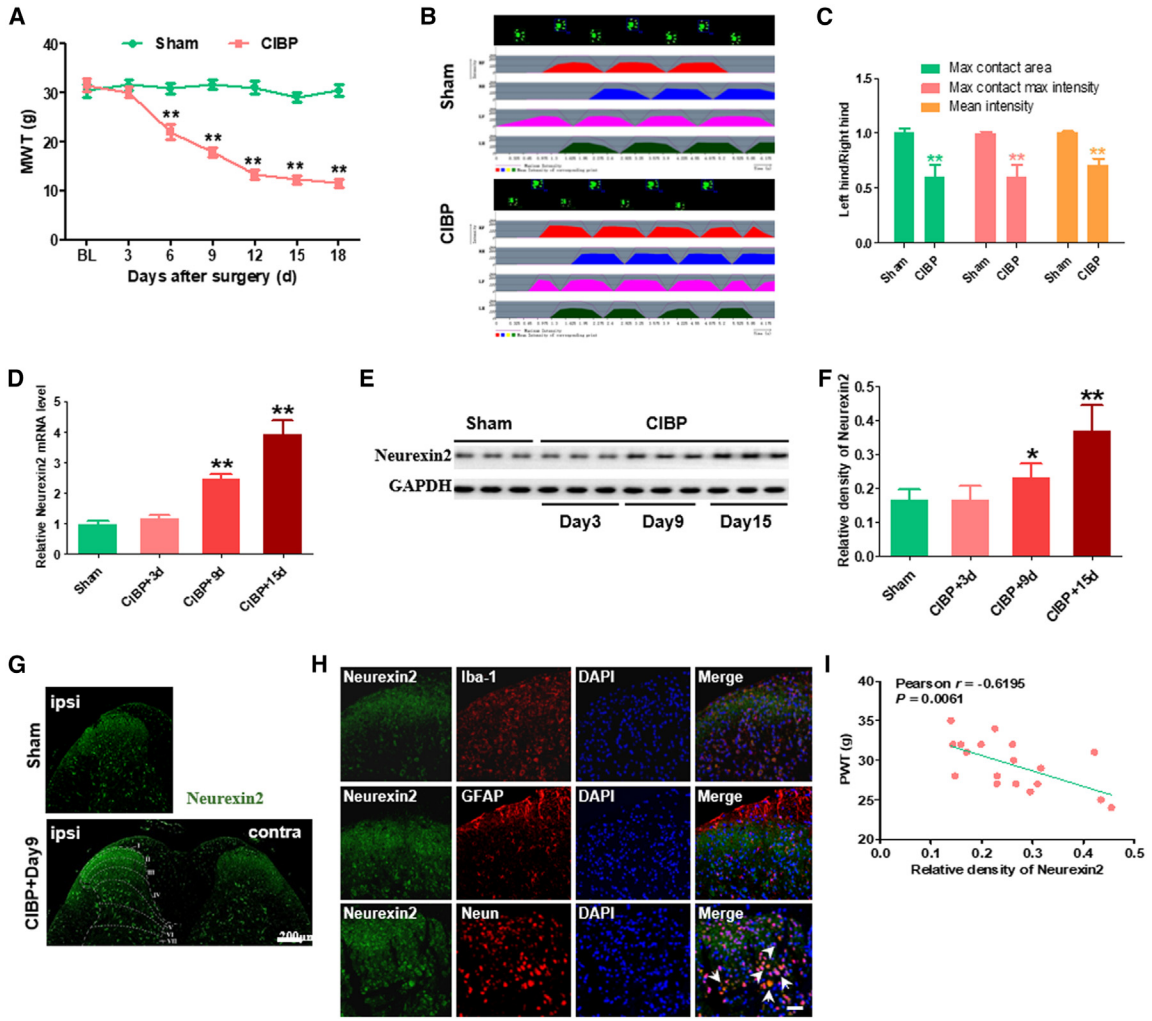

Figure 1. Expression and localization of neurexin 2 in the SDH tissue of rats with CIBP

(A) Reduced mechanical pain thresholds in the hindfoot of CIBP rats on days 6–18 after surgery ($n = 11$). (B) Hindfoot footprint and plantar pressure intensity in both groups of rats from the CatWalk gait test. (C) A significantly lower percentage of ipsilateral (left)/contralateral (right) hindfoot in three selected parameters in CIBP rats as compared with sham rats ($n = 8$). (D) qPCR analysis of neurexin 2 mRNA expression in the sham and CIBP groups at different time points ($n = 6$). (E and F) Western blot analysis of neurexin 2 expression in the sham and CIBP groups at different time points ($n = 6$). (G) Immunofluorescence staining of neurexin 2 (green) in the SDH of the sham and CIBP groups. (H) Neurexin 2 (green) is double fluorescently labeled with Iba1 (red) for microglia, GFAP (red) for astrocytes, and NeuN (red) for neurons. (I) Correlation analysis between pain threshold and neurexin 2 expression in CIBP rats at different time points. Results are expressed as mean ± SEM. Repeated measures with ANOVA or unpaired *t* test; $^{*}p < 0.05$, $^{**}p < 0.01$ as compared with the sham group. LH, left hind paw; RH, right hind paw; MWT, mechanical paw-withdrawal threshold. Scale bar, 100 μm.

group (Figures 2D–2J), indicating that intrathecal injection of neurexin 2-siRNA improved the associated negative emotional behaviors induced by CIBP.

To assess the effect of neurexin 2 knockdown on CIBP-induced neuronal sensitization in the spinal cord, neurexin 2-siRNA or MC-siRNA was intrathecally injected on days 6 and 8 after CIBP modeling. The expression of c-Fos protein (a marker of neuronal sensitization) was detected in the spinal cord on day 9. Immunostaining results revealed a significant increase in the number of c-Fos-positive cells in the ipsilateral spinal cord of rats with CIBP as compared with the sham group, and this increase was suppressed by intrathecal injection of neurexin 2 siRNA (Figures 2K–2L). These findings suggested that the decrease in neurexin 2 expression resulted in the remission of CIBP and may be achieved through the inhibition of spinal cord neuronal sensitization.

Upregulation of neurexin 2 mRNA acetylation expression in the SDH tissue of rats with CIBP

Recently, the study of epigenetics in the mechanism of chronic pain occurrence has become a hotspot[28] and is expected to be one of the molecular etiologies revealing the molecular etiology of CIBP.

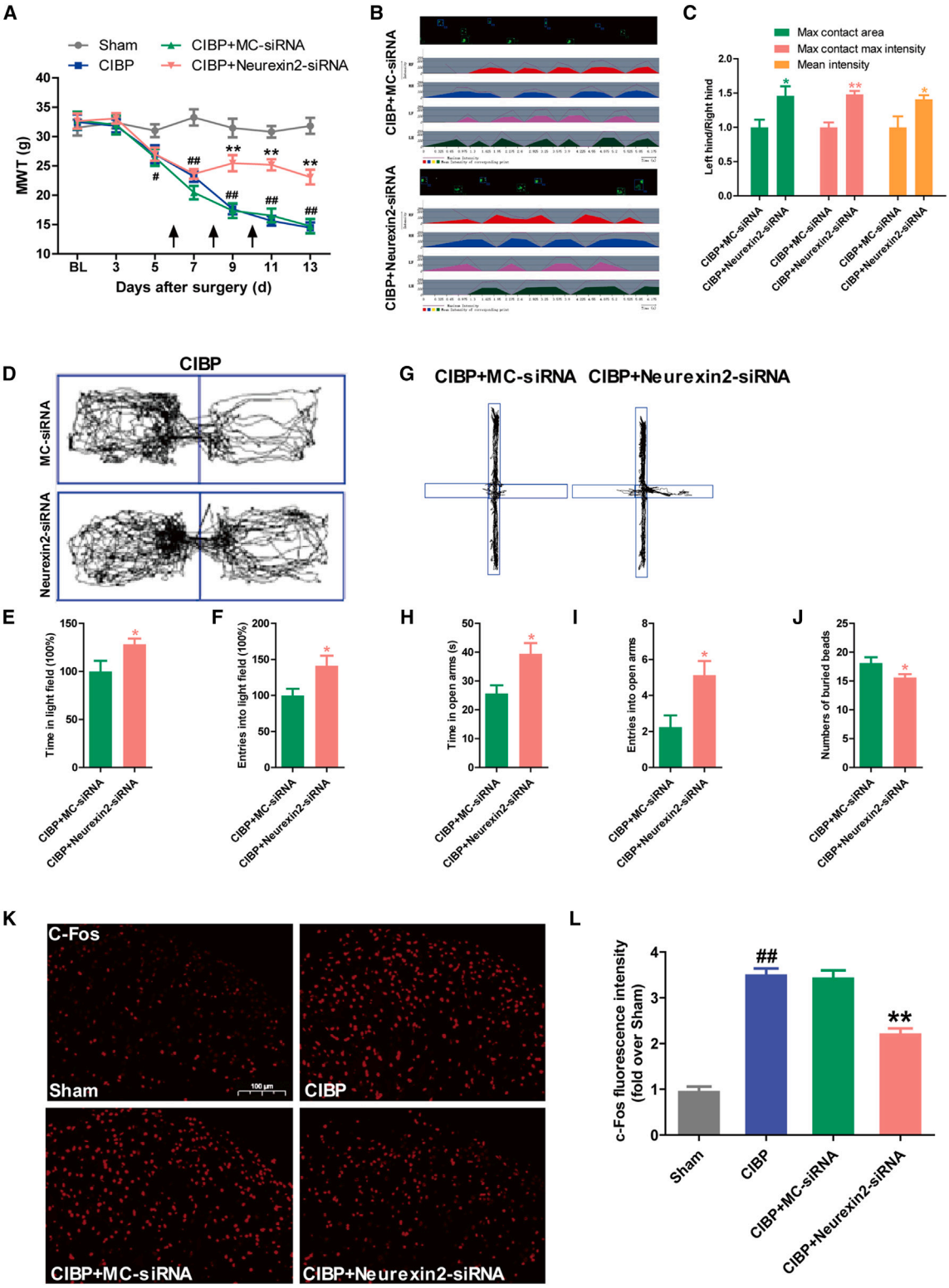

(legend on next page)

N4-acetylcytosine acetylation is a conserved chemical modification that acetylates acetylcytosine at the N4 position in response to the action of RNA ac4C-modifying enzymes.[29] However, the regulation of chronic pain via RNA acetylation has not yet been reported. Our group previously used acRIP-seq to assess the characteristics of transcriptome expression and distribution changes of ac4C in the SDH tissue of CIBP and control rats (Figure 3A).[25] Most ac4C peaks contained different CXX repetitive sequences (Figure 3B). We observed that ac4C was widely distributed in the transcriptome, with most sites occurring within the coding sequence (CDS) and the 3′UTR (Figures 3C and 3D). The two groups of genes with differential ac4C modifications were reported to be involved in the regulation of important biological functions in the rat (Figure 3E). Among the numerous differential gene mRNA acetylation molecules, we found that neurexin 2 mRNA acetylation expression was upregulated in CIBP rats and the CDS region (Figure 3F). Validation by acRIP-qPCR revealed that neurexin 2 mRNA acetylation was upregulated in a time-dependent manner (Figure 3G). Finally, we measured the pain thresholds in CIBP rats before taking spinal cord tissues for acRIP-qPCR assay with the expression of neurexin 2 mRNA acetylation, and we found that they were negatively correlated, such that higher expression of neurexin 2 mRNA acetylation led to a lower pain threshold (Figure 3H).

NAT10-mediated regulation of neurexin 2 mRNA acetylation and expression in the SDH tissue of CIBP rats

To further investigate the role of neurexin 2 mRNA acetylation in the development of CIBP, we focused on the RNA ac4C modifying enzyme NAT10. NAT10 and neurexin 2 were found to be co-expressed on primary cultured neurons from the SDH of Sprague-Dawley rats by immunofluorescence double-labeling assay (Figure 4A). Subsequently, we performed the NAT10-RNA immunoprecipitation-qPCR assay, and the results displayed a significant increase in the percentage of NAT10 binding to neurexin 2 mRNA in the SDH tissue of CIBP rats (Figure 4B).

To investigate the impact of NAT10 on neurexin 2 expression, we designed and modified siRNA oligonucleotides targeting NAT10 and neurexin 2 (NAT10-siRNA and neurexin 2-siRNA, respectively). Intrathecal administration of siRNA was performed on day 6 after modeling in Sprague-Dawley rats, with injections every other day. SDH tissues were collected on day 9 for qPCR and western blot analysis. The results demonstrated an upregulation of NAT10 and neurexin 2 mRNA and protein expressions in the CIBP group as compared with the sham group (Figures 4C–4E). As compared with the CIBP+MC-siRNA group, the mRNA and protein expressions of NAT10 and neurexin 2 were decreased in the CIBP+NAT10-siRNA group (Figures 4C–4E), whereas only neurexin 2 mRNA and protein expressions were decreased in the CIBP+neurexin 2-siRNA group (Figures 4C–4E). Additionally, the acRIP-qPCR assay revealed an upregulation of neurexin 2 mRNA acetylation in the CIBP group as compared with the sham group (Figure 4F) and downregulation of neurexin 2 mRNA acetylation in the CIBP+NAT10-siRNA group as compared with the CIBP+MC-siRNA group (Figure 4F). These findings confirmed that NAT10-siRNA could reverse the upregulation of neurexin 2, neurexin 2 mRNA, and neurexin 2 mRNA acetylation in CIBP rats, thereby highlighting the role of the RNA ac4C-modifying enzyme NAT10 in catalyzing neurexin 2 mRNA acetylation and promoting neurexin 2 protein expression in the SDH tissue of CIBP rats.

Ac4C prolongs neurexin 2 mRNA half-life and regulates neurexin 2 expression

We investigated the relationship between NAT10-induced neurexin 2 mRNA acetylation and neurexin 2 expression in the same CIBP rats from the previous experiments. We found a positive correlation between neurexin 2 mRNA acetylation and neurexin 2 expression, such that higher neurexin 2 mRNA acetylation led to increased neurexin 2 expression (Figure 5A). We further experimented with PC12 cells to understand the regulation between neurexin 2 mRNA acetylation and neurexin 2 expression. The cells were divided into five groups: MC-siRNA group, NAT10-siRNA group, NAT10 inhibitor Remodelin hydrobromide group, NAT10 overexpression (NAT10-OE) group, and NAT10-OE control (NC-OE) group. The expression of NAT10 was verified by qPCR and western blot analysis to confirm the effects of NAT10-siRNA, Remodelin hydrobromide, and NAT10-OE on NAT10 expression in PC12 cells. NAT10 expression was decreased in the NAT10-siRNA and Remodelin hydrobromide groups as compared with the MC-siRNA group (Figures 5B and 5C). Conversely, NAT10 expression was upregulated in the NAT10-OE group as compared with the NC-OE group (Figures 5B and 5C). After culturing and transfecting the cells, we assessed the half-life of neurexin 2 mRNA in each group. We observed that neurexin 2 mRNA had a longer half-life in cells cultured with NAT10-OE as compared with cells cultured with NC-OE, while the half-life of neurexin 2 mRNA was decreased after silencing NAT10 or adding Remodelin hydrobromide (Figure 5D).

Figure 2. Intrathecal injection of neurexin 2-siRNA alleviates Walker-256 breast cancer cell-induced pain behavior and spinal neuron sensitization in CIBP rats

(A) Mechanical pain threshold in the hindfoot of CIBP rats increased after intrathecal neurexin 2-siRNA injection in CIBP rats ($n = 11$). (B and C) Posterior footprint and plantar pressure intensity increased after intrathecal neurexin 2-siRNA injection in CIBP rats by CatWalk gait assay ($n = 8$). (D–F) Increased duration and number of light fields in light and dark shuttle experiments for CIBP rats in the neurexin 2-siRNA group ($n = 8$). (G–I) Increased time and movements spent in the center region of the open field for CIBP rats in the neurexin 2-siRNA group ($n = 8$). (J) The number of buried beads in the bead-burrowing experiment was reduced in CIBP rats in the neurexin 2-siRNA group ($n = 8$). (K and L) Ipsilateral spinal c-Fos expression after posttreatment with neurexin 2-siRNA in CIBP rats on day 9 was detected by immunofluorescence ($n = 3$). Results are expressed as mean ± SEM. Repeated measures with ANOVA or unpaired *t* test; $^{\#}p < 0.05$, $^{\#\#}p < 0.01$ as compared with the sham group; $^{*}p < 0.05$, $^{**}p < 0.01$ as compared with the MC-siRNA group.

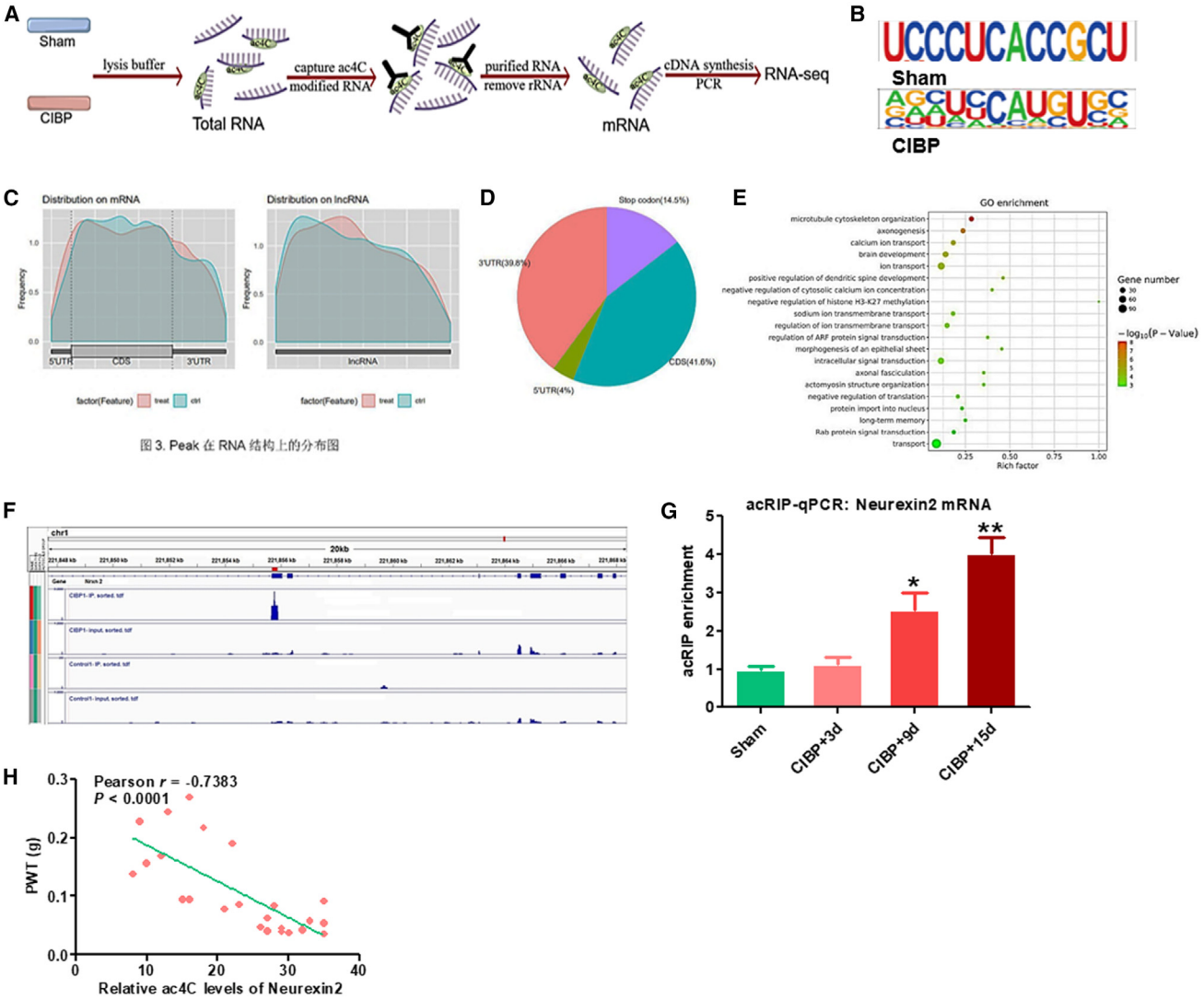

Figure 3. Identification and validation of neurexin 2 mRNA acetylation

(A) Schematic diagram of acRIP-seq, the SDH tissue of rats from the sham and CIBP groups (three biological replicates per group). (B) The ac4C peak motifs expressed in the sham and CIBP groups. (C and D) Percentage distribution of ac4C peaks in acetylated transcripts. (E) Gene ontology enrichment analysis of differentially expressed ac4C peak motifs. (F) AcRIP-seq assay of the neurexin 2 mRNA ac4C site displayed in the CDS region. (G) acRIP-qPCR assay of neurexin 2 mRNA acetylation expression in the sham and CIBP groups at different time points ($n = 6$). (H) Correlation analysis between pain threshold and neurexin 2 mRNA acetylation expression in CIBP rats at different time points. Results are expressed as mean ± SEM. Unpaired t test, $^{*}p < 0.05$, $^{**}p < 0.01$ as compared with the sham group.

Furthermore, we transfected MC-siRNA, NAT10-siRNA, Remodelin hydrobromide, NAT10-OE, and NC-OE in primary cultured neurons from the SDH of Sprague-Dawley rats. We then examined the changes in neurexin 2 mRNA and protein expressions in each group using qPCR and western blot analysis. The results revealed that neurexin 2 mRNA expression was decreased in the NAT10-siRNA and Remodelin hydrobromide groups as compared with the MC-siRNA group. Conversely, neurexin 2 mRNA expression was significantly increased in the NAT10-OE group as compared with the NC-OE group. Consistent with the mRNA results, transfection with NAT10-siRNA resulted in decreased neurexin 2 protein levels as compared with the MC-siRNA control group, while transfection with NAT10-OE led to increased neurexin 2 protein levels as compared with the NC-OE control group (Figures 5E and 5F). In conclusion, our findings revealed that NAT10-induced neurexin 2 mRNA acetylation enhanced the stability of neurexin 2 mRNA and upregulated neurexin 2 expression.

NAT10/ac4C-neurexin 2 axis regulates neuronal synaptogenesis

Neurexins mediate synaptogenesis and have an important role in excitatory synaptic remodeling during pain signaling.[30] To investigate the involvement of the NAT10/ac4C-neurexin 2 axis in excitatory

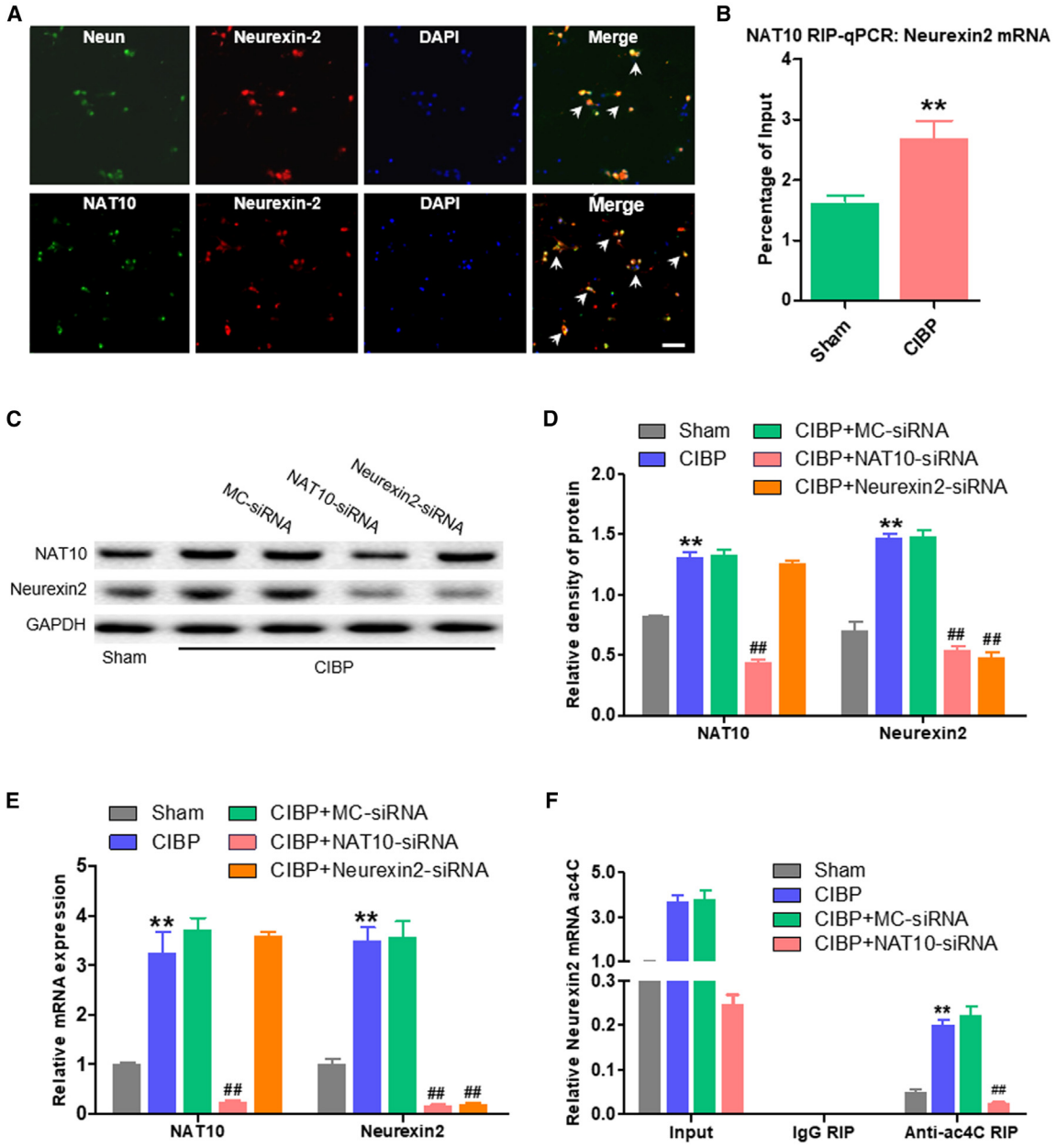

Figure 4. NAT10 regulates neurexin 2 mRNA acetylation and neurexin 2 expression in the SDH tissue of CIBP rats

(A) Multiple fluorescent labeling of neurexin 2 (red) with NeuN (green) and NAT10 (green) in neuronal cells (DAPI, blue) from the SDH of CIBP rats. Scale bar: 40 μm. (B) NAT10-RNA immunoprecipitation (NAT10 RIP)-qPCR detection of neurexin 2 mRNA expression in SDH tissues of rats in the sham and CIBP groups ($n = 6$). (C and D) Western blot of the expressions of NAT10 and neurexin 2 in SDH tissues of CIBP rats, with GAPDH as the internal reference control ($n = 6$). (E) qPCR of NAT10 mRNA and neurexin 2 mRNA expressions in SDH tissues of CIBP rats ($n = 6$). (F) acRIP-qPCR of neurexin 2 mRNA acetylation in SDH tissues of CIBP rats ($n = 6$). Results are expressed as mean ± SEM; unpaired t test, $^{**}p < 0.01$ as compared with the sham group; $^{\#\#}p < 0.01$ as compared with the MC-siRNA group.

synapse formation in the dorsal horn of the spinal cord of CIBP rats, we inhibited the expressions of NAT10 and neurexin 2 using interfering sequences and observed their effects on excitatory synapse formation in the SDH of CIBP rats. Intrathecal administration of siRNA was initiated on day 6 after modeling in Sprague-Dawley rats, with injections every other day. On day 9, spinal cord tissues were collected from the dorsal horn for qPCR, western blot, and immunofluorescence double-labeling analysis. The expression and distribution of the presynaptic membrane marker for excitatory synapses, Syn, and the postsynaptic membrane marker, PSD-95, were

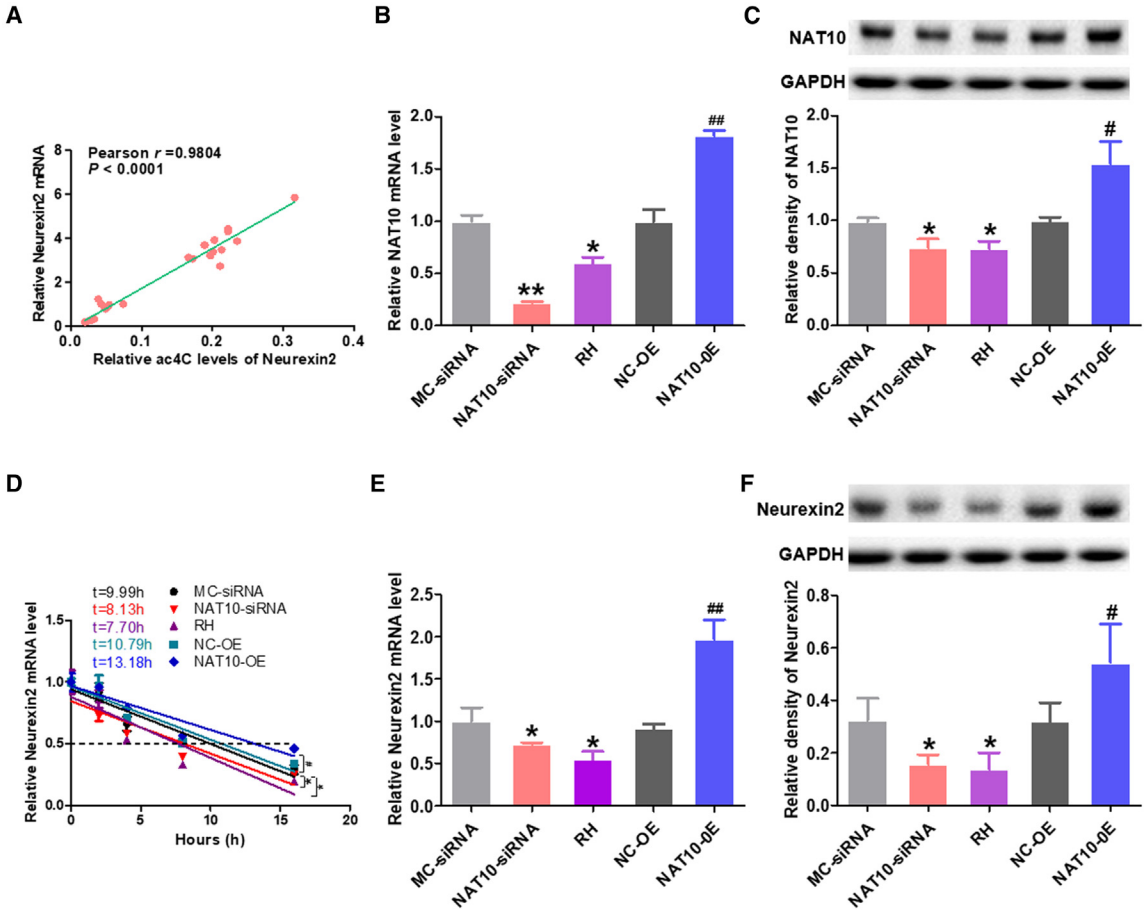

Figure 5. Ac4C regulates the half-life of neurexin 2 mRNA and neurexin 2 expression

(A) Relationship between neurexin 2 mRNA acetylation and neurexin 2 expression. (B) qPCR verifying the effects of NAT10-siRNA, NAT10 inhibitor Remodelin hydrobromide (RH), and NAT10-OE on NAT10 mRNA expression in PC12 cells ($n = 3$). (C) Western blot verifying the effects of NAT10-siRNA, NAT10 inhibitor RH, and NAT10-OE on NAT10 expression in PC12 cells. GAPDH represented the internal reference control ($n = 3$). (D) PC12 cells in five groups were analyzed for the semi-attenuation rate of neurexin 2 mRNA by qPCR at specific time points after treatment with actinomycin D (5 mg/mL) ($n = 3$). (E) qPCR analyzed the effects of NAT10-siRNA, RH, and NAT10-OE on neurexin 2 mRNA expression in primary cultured SDH neurons from Sprague-Dawley rats ($n = 3$). (F) Western blot to analyze NAT10-siRNA, RH, and NAT10-OE on neurexin 2 mRNA expression in primary cultured SDH neurons from Sprague-Dawley rats ($n = 3$). Results are expressed as mean ± SEM; unpaired *t* test, $^{*}p < 0.05$, $^{**}p < 0.01$ as compared with the MC-siRNA group; $^{\#}p < 0.05$, $^{\#\#}p < 0.01$ as compared with the NC-OE group.

examined. Both qPCR and western blot analysis reported upregulated expressions of Syn and PSD-95 on the cell membranes of the SDH tissues of CIBP rats, but transfection with neurexin 2-siRNA or NAT10-siRNA reversed this bone cancer-induced upregulation of Syn and PSD-95 expressions (Figures 6A–6C).

Immunofluorescence double labeling was used to assess the changes and distribution of Syn and PSD-95. The results displayed a significant increase in the number of excitatory synapses in the SDH tissues of CIBP rats as compared with the sham group. However, transfection of neurexin 2-siRNA or NAT10-siRNA reversed the bone cancer-induced increase in excitatory synapses in the SDH of rats (Figures 6D–6G). Furthermore, we examined the effect of the NAT10/ac4C-neurexin 2 axis on synapse formation in the SDH of CIBP rats using electron microscopy. The results suggested that the number of synapses in the SDH of rats was significantly increased in the CIBP group as compared with the sham group. However, transfection of neurexin 2-siRNA or NAT10-siRNA reversed the bone cancer-induced increase in synapse number as compared with the MC-siRNA group (Figures 6H–6J).

Consistent with the *in vitro* transfection experiments, western blot analysis reported that transfection of NAT10, neurexin 2 interfering sequences, and the NAT10 inhibitor Remodelin hydrobromide suppressed the expressions of Syn and PSD-95 in primary cultured neurons from the SDH of Sprague-Dawley rats. Conversely, the overexpression of NAT10 resulted in the upregulation of Syn and PSD-95 expressions (Figures S1A–S1C). Furthermore, in cells transfected

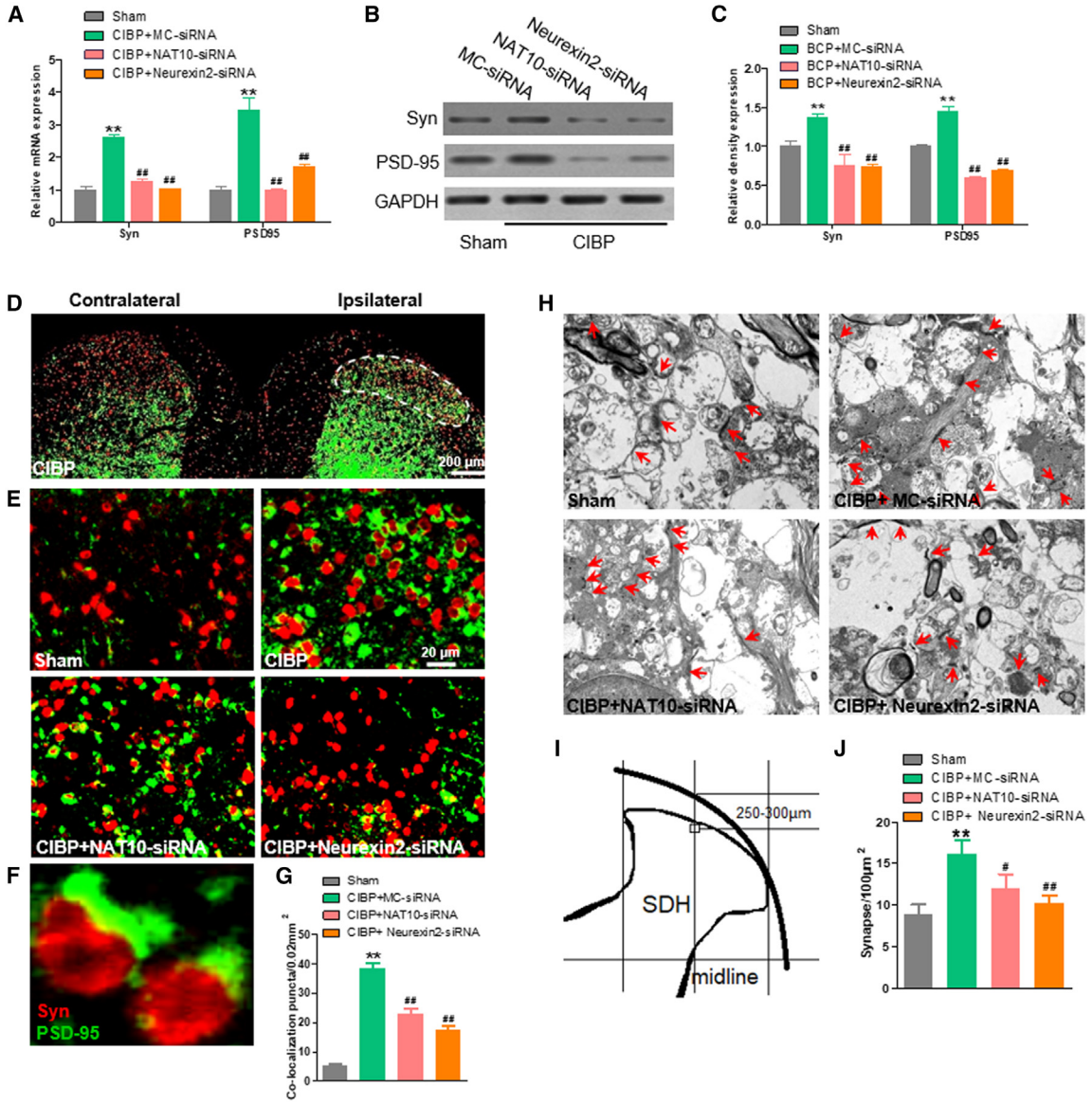

Figure 6. NAT10/ac4C-Neurexin2 axis regulates neuronal synaptogenesis in the SDH of CIBP rats

(A) qPCR analyzed the effects of NAT10-siRNA and neurexin 2 siRNA on the expression of Syn and PSD-95 mRNAs in SDH tissues of CIBP rats ($n = 3$). (B and C) Western blot to analyze the effects of NAT10-siRNA and neurexin 2-siRNA on the expressions of Syn and PSD-95 in SDH tissues of CIBP rats. GAPDH represented the internal reference control ($n = 3$). (D) The expressions of Syn and PSD95 were observed at low magnification and localized (white circle) in the SDH of CIBP rats. (E) Fluorograms of excitatory synapses in the ipsilateral SDH of rats in four groups. (F) Excitatory synapses in the SDH were observed with high magnification, and the points where Syn (red) and PSD95 (green) overlapped were excitatory synapses. (G) Three samples in each group, one slice for each sample, and five fields of view 0.02 mm^2 were randomly taken from each slice. The number of synapses in each field of view was counted, and the mean value was taken as the number of synapses in that sample ($n = 15$). (H) Synapses were observed by transmission electron microscopy in the SDH of rats and marked with red arrows. (I) The synapses were localized and detected under the microscope at a depth of about 250–300 μm in the median line of the dorsal horn of the spinal cord. (J) Three samples in each group, one section per sample. Five fields of view 100 μm^2 were randomly taken from each section. The number of synapses in each field of view was counted, and the mean value was taken as the number of synapses in that sample ($n = 15$). Data are expressed as mean ± SEM; unpaired t test, $^{**}p < 0.01$ as compared with the sham group; $^{\#}p < 0.05$, $^{\#\#}p < 0.01$ as compared with the MC-siRNA group.

with overexpressed NAT10 and then transfected with neurexin 2 interfering sequences, partial inhibition of Syn and PSD-95 expressions was observed as compared with NAT10-OE (Figures S1A–S1C). Immunofluorescence double labeling of spinal cord neurons from primary cultured Sprague-Dawley rats was performed to assess the co-localization of Syn with PSD-95. The number of excitatory synapses was determined by the relative fluorescence values of Syn and PSD-95. Transfection of NAT10, neurexin 2 interfering

sequence, and Remodelin hydrobromide inhibited the relative fluorescence values of Syn and PSD-95, while the relative fluorescence values of Syn and PSD-95 were upregulated in cells transfected with overexpressed NAT10 (Figures S1D–S1F). When NAT10-overexpressing cells were transfected with neurexin 2 interfering sequences, the relative fluorescence values of Syn and PSD-95 were downregulated as compared with NAT10-OE (Figures S1D–S1F).

These experimental findings demonstrated that the NAT10/ac4C-neurexin 2 axis could be involved in bone cancer-induced excitatory synapse formation in the SDH of rats, which could contribute to CIBP development.

DISCUSSION

This study identified and validated, for the first time, the role and mechanism of neurexin 2 in the formation of CIBP, which may be one of the potential key target molecules for the treatment of CIBP. In a rat model of CIBP, a significant increase in neurexin 2 expression in SDH neurons and the epigenetic mechanism leading to the increase were identified, revealing that NAT10 regulated neurexin 2 mRNA acetylation modification and neurexin 2 expression. Knockdown of spinal neurexin 2 expression by interfering RNA confirmed the regulatory role of neurexin 2 in pain behavior and spinal neuron sensitization in CIBP rats. In addition, the NAT10/ac4C-neurexin 2 axis was found to modulate excitatory glutamate receptor function and neuronal synaptogenesis. In conclusion, the findings suggested that NAT10 in spinal cord neurons of CIBP rats enhanced neurexin 2 mRNA acetylation modification, improved mRNA stability, and promoted the expression of neurexin 2. Likewise, the upregulated neurexin 2 expression led to the remodeling of spinal synapses and the development of conscious hypersensitivity in CIBP.

CIBP is the most persistent and common clinical complication of advanced cancer, occurring in 70% of patients with advanced breast cancer and 40% of patients with advanced lung cancer,[31] thereby greatly affecting patients' quality of life and survival time.[32] Due to the lack of effective treatments, most pain management specialists believe that the primary pain treatment for CIBP is opioid therapy, which contrarily has unavoidable serious adverse effects.[32] Therefore, there is an urgent need to develop new treatments for CIBP.

The CIBP model was made by injecting Walker 256 cells into the tibia of rats. The Walker 256 cell line is a type of breast cancer cell, so female Sprague-Dawley rats were selected. Walker-256 tumor cells were first discovered in 1928 by Dr. George Walker in the breasts of pregnant albino rats and are considered to be carcinosarcomas,[33] which are among the most widely used transplantable tumors in experimental research. Walker-256 cells at the implantation site in rats caused significant bone resorption and increased skeletal fragility, which is consistent with the phenotype seen in breast cancer patients who have developed bone metastases. To maintain the homology and compatibility of the implanted cells with the host animal, an experimental animal model of intraosseous breast cancer was established that highly mimicked the human disease,[34] and female rats were used in this study because breast cancer is more commonly seen in females. Although differences in the estrus period were observed between the sexes, these differences were small and did not affect the overall progression of CIBP status.[35]

The neurexin family of proteins is a highly polymorphic class of cell adhesion molecules specifically expressed in mammalian neurons (at the presynaptic membrane) and bind to the receptor neuroligins (at the postsynaptic membrane), as well as other proteins.[36] Recently, neurexins and their binding proteins at the postsynaptic membrane have received increasing attention from researchers, as variants of both have been associated with a variety of neurological and psychiatric disorders.[37] In the present study, we found that the expression of neurexin 2 gradually increased with the progression of CIBP and was positively correlated with the pain threshold in CIBP. Further experiments revealed that decreasing neurexin 2 expression not only inhibited the decrease of pain threshold in CIBP rats but also inhibited the sensitization of SDH neurons. This finding suggested that the dysregulation of neurexin 2 expression is involved in CIBP formation.

Neurexin 2 is also involved in the mechanism of nociceptive sensitization in rats with bone cancer. In the central nervous system, excitatory synaptic transmission of transmitters dominated by glutamate acts on postsynaptic glutamate receptors,[38] converting presynaptic electrical signals into Ca^{2+} signals within the postsynaptic neuron and initiating a series of biochemical cascade reactions that lead to plastic changes in the synapse.[39] Through the utilization of electron microscopy and molecular biology techniques, our investigation revealed that NAT10/ac4C-neurexin 2 pathway regulated synaptic morphology and the expression of synapse-associated proteins within SDH of CIBP rats. Consequently, the synapse is expected to undergo structural remodeling, leading to consequential modifications in synaptic transmission efficiency. Over the past decade, a substantial body of experimental evidence has consistently demonstrated that spinal synaptic plasticity serves as the underlying mechanism for central sensitization of pain and the foundation for nociceptive hypersensitivity.[40]

Having clarified the role and possible mechanisms of neurexin 2 in CIBP, targeting the modulation of neurexin 2 expression may be a potential treatment for bone cancer-induced hypersensitivity reactions. In the development of numerous diseases, a growing body of research suggests that epigenetics plays an important role. Studies have also reported that epigenetic alterations are equally important in the modulation of nociceptive information in tissue injury or inflammation and that pain-induced epigenetic alterations are a reversible process.[41,42] Consequently, restoration of aberrant epigenetic morphology in the pain transmission pathway could theoretically alleviate pain and inhibit the development of chronic pain. Numerous compounds acting on epigenetic modification systems are effective against cancer cells, such as the histone deacetylase inhibitor hydroxamic acid, which was approved by the U.S. Food and Drug Administration.[43] The initial success of epigenetic therapies for cancer treatment lays the groundwork for investigating similar approaches to address

chronic pain, which would be a novel approach distinct from traditional pain symptom treatments.

Epitranscriptomics focuses on modifying the structure and function of RNAs through post-transcriptional modifications and has been one of the cutting-edge research areas in biomedicine in the last few years.[6,44,45] N4-acetylcytosine acetylation is the acetylation of cytosine at position N4 in the presence of RNA ac4C-modifying enzymes.[8] In the field of covalent modification of proteins, studies have suggested that acetylation/deacetylation is the second most important covalent modification factor, which is closely related to pain and functions as post-transcriptional regulators.[10,46,47] However, not many studies have reported the modulation of chronic pain by RNA acetylation. In this study, acRIP-seq assay revealed that ac4C was widely distributed in the SDH L4–L6 transcriptome, with most sites occurring within the CDS. By correlating the mRNA ac4C differential genes with the mRNA expression differential genes in control and bone cancer rats, numerous genes were found to be significantly different from each other, which suggested that mRNA ac4C may play an important role in CIBP formation. Through further in-depth analysis of the data detected by acRIP-seq, we found that the expression of neurexin 2 mRNA ac4C was also altered and that neurexin 2 mRNA acetylation was upregulated in a time-dependent manner. Correlation analysis of pain thresholds in CIBP rats and the expression of neurexin 2 mRNA acetylation revealed that they were negatively correlated. We studied the dysregulation of NAT10 and found that the half-life of neurexin 2 mRNA was prolonged in neuronal cells overexpressing NAT10 and shortened in neuronal cells inhibiting NAT10 expression. *In vitro* and cytological experiments further verified that inhibition of NAT10 suppressed neurexin 2 expression. This finding suggested that ac4C participates in the formation of CIBP by regulating neurexin 2.

Our study has elucidated the role of neurexin 2 in the development of CIBP through its modulation of synaptic plasticity. Additionally, we highlighted the significance of spinal ac4C modification in the post-transcriptional regulation of neurexin 2 in CIBP. Therefore, targeting neurexin 2 ac4C through epigenetic interventions holds promise as a potential therapeutic strategy for CIBP, as it does not interfere with the normal functioning of the nervous system. Consequently, our findings established the theoretical foundation for developing innovative and efficacious therapeutic agents for managing cancer pain.

MATERIALS AND METHODS

Experimental animals

Female Sprague-Dawley rats at 6 weeks of age with an average weight of 200 ± 20 g were procured from Zhejiang Vital River Laboratory Animal Technology Co., Ltd. (Production License: SCXK(Zhe) 2019-0001). The rats were housed in specific pathogen-free chambers with ad libitum access to food and water at a controlled temperature of 21°C–23°C. The rats were allowed to acclimatize to the experimental environment for 2 days before the commencement of the study. Consistent with previous investigations,[48–50] the rats were anesthetized using 5 mg/mL sodium pentobarbital. All animal experiments were conducted within the time frame of 8:00 AM to 8:00 PM. Given that the objective of this study was to assess the chronic pain status, analgesics were not administered during the behavioral assessment to avoid any potential interference with the experimental outcomes. The animal experiments in this study were approved by the Institutional Animal Care and Use Committee of Jiaxing College (Ethical Approval No. JUMC2020-018). They were performed in accordance with the ethical standards outlined in the Declaration of Helsinki and the Declaration of the International Society for the Study of Animal Pain.

Establishment of the CIBP model

Under microscopic observation, Walker-256 cells (1×10^6 cells/mL) and heat-inactivated Walker-256 cells (sham-operated group) were prepared. Female Sprague-Dawley rats weighing 200 ± 10 g were anesthetized using sodium pentobarbital (50 mg/kg, intraperitoneally). A longitudinal incision of approximately 5 mm was made on the medial side of the upper end of the left tibia, and a No. 5 syringe needle was used to puncture the incision at a 45° angle toward the metaphysis, creating a hole. Subsequently, a 10 μL suspension of cancer cells was extracted using a microsyringe and injected into the bone marrow cavity at a slow and constant rate. After a 30-s interval, the syringe was withdrawn, and the bone was closed using medical bone wax. The incision was sterilized with povidone-iodine and sealed with biomedical adhesive. In the entire study, different cohort animals were used for each test.

siRNA transfection

The NAT10-siRNA, neurexin 2-siRNA, and mismatch control siRNA (MC-siRNA) were chemically synthesized by Guangzhou RiboBio Biotechnology Co. Primary cultured SDH neurons from Sprague-Dawley rats were co-transfected with siRNA using Lipofectamine 2000. After 48 h, the knockdown effect of siRNA was evaluated by measuring the mRNA expression of the targeted genes using qPCR. The NAT10-siRNA (5′-CCTTACTCCTCCAAGTTGAA-3′), neurexin 2-siRNA (5′-CGACGAGGGCUCCUACCAAdTdT-3′), and MC-siRNA (5′-UCGCCUGAACUCUAGCUGA-3′), which exhibited the highest inhibitory effect, were selected for modification with 5′ Chol +2′ OMe and intrathecal administration to rat L4–L6 SDH. The siRNA administration involved a dose of 3 nmol at 1-day intervals, starting on day 6 after establishing the CIBP model.

Behavioral assessments

Von Frey test

Pain behavior was assessed using calibrated Von Frey monofilaments (BME-404, Institute of Biomedical Sciences, Chinese Academy of Medical Sciences). Female Sprague-Dawley rats from the Jiaxing College Laboratory Animal Center were placed in a plexiglass chamber for 2 days of training before behavioral evaluation. Monofilaments were applied to the plantar surface of the hind paw until a positive response (paw retraction or foot licking) was observed. The average of five consecutive measurements represented the mechanical withdrawal threshold.

Gait analysis

The gait of experimental rats was analyzed using the CatWalk XT system (AsterWee Information Technology). Rats walked on a closed sidewalk with a glass plate, and their movements were recorded and analyzed. A camera mounted beneath the device captured paw prints as rats walked across the glass floor. Parameters, such as maximum contact area, maximum contact maximum intensity, and average intensity, were used to assess dynamic behavior associated with CIBP. Left hind claw/right hind claw was used to eliminate confounding factors. Data were expressed as percentages of ipsilateral/contralateral hindpaw.

Elevated cross maze test

The elevated cross maze consisted of two open arms and two closed arms. Rats were placed in the middle area facing the open arms, and their movements were recorded for 6 min. The number of entries into the open arms and the time spent in the open arms were recorded as indicators of negative emotional behavior.

Light and dark shuttle experiment

Light and dark boxes were divided into two chambers, with the light-box occupying one-half of the space and the dark box occupying the other one-half. A small door allowed rats to shuttle freely between the chambers. Rats were placed in the dark box and allowed to explore for 6 min. The time and number of entries into the bright field were recorded as indicators of negative emotional behavior.

Buried strain experiment

Rats were placed in standard-sized cages with a layer of bedding and evenly distributed glass beads. After 30 min, the number of buried beads was observed. Burial was defined as more than two-thirds of the glass beads being buried. The number of buried beads was recorded as an indicator of anxiety level.

Primary cell culture

Fresh spinal cord tissue was obtained from three-day-old Sprague-Dawley rats, and the cells were suspended in serum-free DMEM/F12 by centrifugation at 1,000 rpm for 5 min after grinding, digestion, and filtration and then transferred to a medium containing 10% fetal bovine serum. Cells were diluted to 1×10^6 cells/mL and then placed in culture at 37°C, 95% air, and 5% CO_2. After 3 days, cytarabine (10 M) was added to the medium to reduce glial cell proliferation for purification. The cell culture medium was changed daily, and neuronal cell growth was observed.

Western blot

To quantify the proteins, the SDH tissue was lysed using a method described in a previous report. The protein concentration was determined using the enhanced BCA protein assay kit. Approximately 30 μg of protein samples were separated by electrophoresis on a 10% SDS-PAGE gel and transferred onto a PVDF membrane. The membrane was then incubated with specific antibodies against the proteins of interest, as listed in Table S1. After blocking with 10% skim milk, the membrane was incubated with GAPDH antibody overnight at 4°C with continuous shaking. The membrane was then rinsed with PBS three times. Colorimetric detection was performed using the ECL western Blotting Detection Kit (Millipore). Finally, the protein bands were quantified using the ImageJ software. For the detection of synaptophysin (Syn) and PSD-95 proteins, neuronal cell membranes were extracted using the Mem-PER Plus Kit (Invitrogen, item no. 89842) and subjected to western blot analysis.

Real-time fluorescence qPCR

Total RNA was extracted from fresh rat spinal cord tissue using Trizol reagent from Invitrogen. For the isolation of total neuronal RNA, the Cytoplasmic and Nuclear RNA Purification Kit from Invitrogen was used according to the manufacturer's instructions. The PCR reaction was performed with a 20 μL solution consisting of PCR master mix from Fermentas (K0171), forward and reverse primers, and diluted cDNA. The primer sequences for amplification of the target genes are listed in Table S2. The annealing temperature was set at 53°C. Real-time qPCR amplification was performed using the Rotor-Gene QTAMRA 1109 Sequence Detection System from Qiagen. The reaction conditions included an initial polymerase activation step at 95°C for 2 min, followed by 40 cycles of denaturation at 95°C for 15 s, annealing at 53°C for 20 s, and extension at 60°C for 30 s for amplification and signal collection. The expression levels of the target genes were normalized using GAPDH, and the $^{\Delta\Delta}$Ct method was employed to assess differential expression.

Immunofluorescence

Cells were fixed with 4% paraformaldehyde and permeabilized with 0.5% Triton X-100 in PBS for 20 min. The cells were then blocked with serum for 2 h at room temperature. For the processing of spinal cord tissue, the spinal cords were rapidly isolated and post-fixed with 4% paraformaldehyde. Then, they were dehydrated with a 30% sucrose solution. The spinal cord was cut into 20-μm sections, and the sections were permeabilized with 0.3% Triton X-100 and blocked with 5% standard fetal bovine serum for 1 h at room temperature. Next, the sections were incubated overnight at 4°C with the target protein 1 antibody. Subsequently, fluorescent (Cy3)-labeled goat anti-mouse IgG secondary antibodies were added, and the cells were blocked with serum for 2 h at room temperature. Target protein 2 antibodies were added to the cells and incubated overnight at 4°C. Finally, a fluorescent (fluorescein isothiocyanate)-labeled goat anti-rabies IgG secondary antibody was added, and the cells were incubated in a humid chamber at 20°C–37°C for 1 h. DAPI was added to the cells as a counterstain and incubated in the dark for 5 min. The slides were mounted using an anti-fluorescent mounting agent, and images were captured under a fluorescence microscope (CKX41SF, Olympus, Japan). The details of the antibodies used for the target proteins are listed in Table S3.

acRIP-qPCR and NAT10RIP-qPCR

acRIP and NAT10-RIP were performed using the RNA Immunoprecipitation Kit (P0101; Geneseed). Total RNA was extracted from rat right side SDH tissues through liquid nitrogen grinding, lysis, and

centrifugation. The following antibodies were mixed with protein A/G beads and incubated at 4°C for 2 h: anti-N4-acetylcytidine antibody (1:50; Abcam, cat. no ab252215), anti-NAT10 (1:50; Proteintech, cat. no 13365-1-AP), rabbit IgG (1:50, 2729S; Cell Signaling Technology), or mouse IgG (1:50, 12–371; Merck Millipore). The beads were then incubated with lysis buffer at 4°C for 2 h. After washing the beads with buffer, RNA was extracted. The neurexin 2 mRNA was detected using real-time qPCR with the following primers: forward (5′–3′): CCTCCTGGCCAACCTGAAG; and reverse (5′–3′): CTTCACTGCAGAACTTGCCG.

NAT10-OE vector construction

To construct the NAT10-OE vector, rat NAT10 sequence fragments and the vector plasmid pLKO.1-puro were prepared. PCR target bands were designed using the following primers: forward (5′–3′): CACCGGTATGCATCGGAAGAAGG; and reverse (5′–3′): CGACGCGTCTACTTCTTTCTCTTCAG. The gum recovery products and vector plasmid pLKO.1-puro were double digested with Age I and Mlu I. The target products were then subjected to gum recovery and purification experiments. The rat Nat10 sequence fragment was ligated to the vector and transformed into *E. coli* HB101 sensory cells. Single colonies were picked and inoculated into an LB liquid medium containing 100 mg/lamp and incubated overnight. Plasmid DNA was prepared using SDS alkaline lysis and subjected to Bam Hl and Hind III double digestion and sequencing. The plasmid was extracted from the bacterial precipitate and stored at −20°C. Product quality inspection was performed after that.

RNA stability assay

PC12 cells were transfected and divided into groups. Each group was then inoculated in 12-well plates and treated with actinomycin D (5 mg/mL; Catalog #HY-17559; Sigma) for varying durations (0, 2, 4, 8, and 16 h). Total RNA was collected from each group separately for subsequent quantitative real-time qPCR analysis. The mRNA half-life was estimated using linear regression analysis.

Transmission electron microscopy of SDH synapses

After the inhalation of sevoflurane anesthesia, the head was swiftly severed, and the L4–L6 spinal cord was immediately removed and cut into 1 mm × 1 mm × 1 mm tissue blocks from the right side SDH region. These tissue blocks were then fixed in a 2.5% glutaraldehyde solution at 4°C for 24 h. The fixed tissue was rinsed in 0.1 mol/L phosphate buffer, further fixed in 1% osmic acid, dehydrated using a gradient of acetone, and embedded in epoxy dendritic acid-618. Semithin sections (1 μm thick) were prepared and positioned, followed by the cutting of ultrathin sections. The sections were stained with saturated uranyl acetate for observation under the electron microscope. The synaptic structural parameters were measured using the Image-pro plus 6.0 image analysis system.

Statistical data

All data obtained in this study were analyzed using GraphPad Prism (version 9.0). The Shapiro-Wilk test confirmed that all experimental values were normally distributed. Results are expressed as the mean ± SEM. Two-way repeated measures ANOVA with Bonferroni *post hoc* test was performed to analyze the pain behavior test results at different time points. Student's *t* test was used to compare experimental results between two groups, while one-way ANOVA with the Student-Newman-Keuls *post hoc* test was used to analyze differences in experimental results between multiple groups. A significance level of $p < 0.05$ was considered statistically significant.

DATA AND CODE AVAILABILITY

All data supporting the findings of this study are available within the article or will be made available from the authors upon request.

SUPPLEMENTAL INFORMATION

Supplemental information can be found online at https://doi.org/10.1016/j.omtn.2024.102200.

ACKNOWLEDGMENTS

The study was supported, in part, by grants from the Natural Science Foundation of Zhejiang Province (LTGC23H090002), National Natural Science Foundation of China, China (82001176), People's Livelihood Science and Technology Innovation Research Project of Jiaxing City, China (2023AY31025), Medical and Health Research Project of Zhejiang Province, China (2023KY1195), Zhejiang Multidisciplinary Innovation Team of Traditional Chinese Medicine for Diagnosis and Treatment of Elderly Headache and Vertigo, China (2022-19), Clinical Key Specialties of Zhejiang Province -Anesthesiology, China (2023-ZJZK-001) and National Clinical Key Specialties-Oncology, China (2023-GJZK-001). We thank Home for Researchers editorial team (www.home-for researchers.com) for language editing service.

AUTHOR CONTRIBUTIONS

Project investigation and experimental design contributed by L.X. (dominated) and M.Y.; experiments contributed by S.Z. (dominated) and L.C., L.Y., S.Z., B.L., K.S., and Q.F.; manuscript writing contributed by L.X. (dominated) and Q.Z.; data visualization contributed by L.X. (dominated), L.Y., and Q.H.; resource management and project direction contributed by L.X. (dominated), Q.H., and M.Y.

DECLARATION OF INTERESTS

The authors declare no competing interests.

REFERENCES

1. Lianos, G.D., Christodoulou, D.K., Katsanos, K.H., Katsios, C., and Glantzounis, G.K. (2017). Minimally Invasive Surgical Approaches for Pancreatic Adenocarcinoma: Recent Trends. J. Gastrointest. Cancer *48*, 129–134.

2. Shi, Y., and Hu, F.B. (2014). The global implications of diabetes and cancer. Lancet *383*, 1947–1948.

3. Arthur, J.A., Tang, M., Lu, Z., Hui, D., Nguyen, K., Rodriguez, E.M., Edwards, T., Yennurajalingam, S., Dalal, S., Dev, R., et al. (2021). Random urine drug testing among patients receiving opioid therapy for cancer pain. Cancer *127*, 968–975.

4. Zhu, C., Zhong, W., Gong, C., Chen, B., and Guo, J. (2023). Global research trends on epigenetics and neuropathic pain, A bibliometric analysis. Front. Mol. Neurosci. *16*, 1145393.

5. Nirvanie-Persaud, L., and Millis, R.M. (2022). Epigenetics and Pain, New Insights to an Old Problem. Cureus *14*, e29353.

6. Malbec, L., Zhang, T., Chen, Y.S., Zhang, Y., Sun, B.F., Shi, B.Y., Zhao, Y.L., Yang, Y., and Yang, Y.G. (2019). Dynamic methylome of internal mRNA N(7)-methylguanosine and its regulatory role in translation. Cell Res. *29*, 927–941.

7. Boccaletto, P., Stefaniak, F., Ray, A., Cappannini, A., Mukherjee, S., Purta, E., Kurkowska, M., Shirvanizadeh, N., Destefanis, E., Groza, P., et al. (2022). MODOMICS, a database of RNA modification pathways. 2021 update. Nucleic Acids Res. *50*, D231–D235.

8. Arango, D., Sturgill, D., Alhusaini, N., Dillman, A.A., Sweet, T.J., Hanson, G., Hosogane, M., Sinclair, W.R., Nanan, K.K., Mandler, M.D., et al. (2018). Acetylation of Cytidine in mRNA Promotes Translation Efficiency. Cell *175*, 1872–1886.e24.

9. Zhang, Y., Lei, Y., Dong, Y., Chen, S., Sun, S., Zhou, F., Zhao, Z., Chen, B., Wei, L., Chen, J., and Meng, Z. (2024). Emerging roles of RNA ac4C modification and NAT10 in mammalian development and human diseases. Pharmacol. Ther. *253*, 108576.

10. Qi, F., Zhou, Y., Xiao, Y., Tao, J., Gu, J., Jiang, X., and Xu, G.Y. (2013). Promoter demethylation of cystathionine-beta-synthetase gene contributes to inflammatory pain in rats. Pain *154*, 34–45.

11. Liang, L., Lutz, B.M., Bekker, A., and Tao, Y.X. (2015). Epigenetic regulation of chronic pain. Epigenomics *7*, 235–245.

12. Medina-Samamé, A., Paller, É., Bril, M.R., Archvadze, A., Simões-Abade, M.B.C., Estañol-Cayuela, P., and LeMaoult, C. (2023). Role of Neurexins in Alzheimer's Disease. J. Neurosci. *43*, 4194–4196.

13. Cheung, A., Konno, K., Imamura, Y., Matsui, A., Abe, M., Sakimura, K., Sasaoka, T., Uemura, T., Watanabe, M., and Futai, K. (2023). Neurexins in serotonergic neurons regulate neuronal survival, serotonin transmission, and complex mouse behaviors. Elife *12*, e85058.

14. Dean, C., and Dresbach, T. (2006). Neuroligins and neurexins, linking cell adhesion, synapse formation and cognitive function. Trends Neurosci. *29*, 21–29.

15. Lee, S.J., Uemura, T., Yoshida, T., and Mishina, M. (2012). GluRdelta2 assembles four neurexins into trans-synaptic triad to trigger synapse formation. J. Neurosci. *32*, 4688–4701.

16. Luo, F., Sclip, A., Jiang, M., and Südhof, T.C. (2020). Neurexins cluster Ca(2+) channels within the presynaptic active zone. EMBO J. *39*, e103208.

17. Südhof, T.C. (2001). alpha-Latrotoxin and its receptors, neurexins and CIRL/latrophilins. Annu. Rev. Neurosci. *24*, 933–962.

18. Klatt, O., Repetto, D., Brockhaus, J., Reissner, C., El Khallouqi, A., Rohlmann, A., Heine, M., and Missler, M. (2021). Endogenous beta-neurexins on axons and within synapses show regulated dynamic behavior. Cell Rep. *35*, 109266.

19. Missler, M., Zhang, W., Rohlmann, A., Kattenstroth, G., Hammer, R.E., Gottmann, K., and Südhof, T.C. (2003). Alpha-neurexins couple Ca2+ channels to synaptic vesicle exocytosis. Nature *423*, 939–948.

20. Hata, Y., Davletov, B., Petrenko, A.G., Jahn, R., and Südhof, T.C. (1993). Interaction of synaptotagmin with the cytoplasmic domains of neurexins. Neuron *10*, 307–315.

21. Sugita, S., Saito, F., Tang, J., Satz, J., Campbell, K., and Südhof, T.C. (2001). A stoichiometric complex of neurexins and dystroglycan in brain. J. Cell Biol. *154*, 435–445.

22. Xu, L., Wang, S., Zhang, L., Liu, B., Zheng, S., and Yao, M. (2022). Cobratoxin Alleviates Cancer-Induced Bone Pain in Rats via Inhibiting CaMKII Signaling Pathway after Acting on M4 Muscarinic Cholinergic Receptors. ACS Chem. Neurosci. *13*, 1422–1432.

23. Ni, H., Xu, M., Kuang, J., Xu, C., He, Q., Luo, G., Fu, J., Zhu, J., Ni, C., Zhao, B., et al. (2023). Upregulation of LncRNA71132 in the spinal cord regulates hypersensitivity in a rat model of bone cancer pain. Pain *164*, 180–196.

24. Fu, J., Zhao, B., Luo, G., Ni, H., Xu, L., He, Q., Xu, M., Xu, C., Wang, Y., Ni, C., and Yao, M. (2023). JAG-1/Notch signaling axis in the spinal cord contributes to bone cancer pain in rats. J. Neurochem. *166*, 747–762.

25. Xu, L., Zheng, S., Liu, B., Xu, C., Yang, L., Zhou, Q., Yao, M., and Li, X.Y. (2023). Epitranscriptomic profiling of N4-acetylcytidine-related RNA acetylation in the spinal dorsal horn of rat with cancer-induced bone pain. Mol. Pain *19*. 17448069231178487.

26. Fu, Q., Huang, X., Wan, S., Li, Y., Li, X., Su, S., Xu, X., and Wu, Y. (2022). P-Rex2 mediation of synaptic plasticity contributes to bone cancer pain. Mol. Pain *18*. 17448069221076460.

27. Liu, J., Misra, A., Reddy, M.V.V.V.S., White, M.A., Ren, G., and Rudenko, G. (2018). Structural Plasticity of Neurexin 1alpha, Implications for its Role as Synaptic Organizer. J. Mol. Biol. *430*, 4325–4343.

28. Giordano, R., Kjær-Staal Petersen, K., and Arendt-Nielsen, L. (2022). The link between epigenetics, pain sensitivity and chronic pain. Scand. J. Pain *22*, 664–666.

29. Zhou, D., Zhai, C., and Xuan, X. (2013). Molecular structure and vibrational spectra of N4-acetylcytosine. Spectrochim. Acta Mol. Biomol. Spectrosc. *112*, 139–145.

30. Levinson, J.N., Chéry, N., Huang, K., Wong, T.P., Gerrow, K., Kang, R., Prange, O., Wang, Y.T., and El-Husseini, A. (2005). Neuroligins mediate excitatory and inhibitory synapse formation, involvement of PSD-95 and neurexin-1beta in neuroligin-induced synaptic specificity. J. Biol. Chem. *280*, 17312–17319.

31. Hird, A., Chow, E., Zhang, L., Wong, R., Wu, J., Sinclair, E., Danjoux, C., Tsao, M., Barnes, E., and Loblaw, A. (2009). Determining the incidence of pain flare following palliative radiotherapy for symptomatic bone metastases, results from three canadian cancer centers. Int. J. Radiat. Oncol. Biol. Phys. *75*, 193–197.

32. Takei, D., and Tagami, K. (2023). Management of cancer pain due to bone metastasis. J. Bone Miner. Metab. *41*, 327–336.

33. Mao-Ying, Q.L., Zhao, J., Dong, Z.Q., Wang, J., Yu, J., Yan, M.F., Zhang, Y.Q., Wu, G.C., and Wang, Y.Q. (2006). A rat model of bone cancer pain induced by intra-tibia inoculation of Walker 256 mammary gland carcinoma cells. Biochem. Biophys. Res. Commun. *345*, 1292–1298.

34. Shenoy, P.A., Kuo, A., Vetter, I., and Smith, M.T. (2016). The Walker 256 Breast Cancer Cell- Induced Bone Pain Model in Rats. Front. Pharmacol. *7*, 286.

35. Lewis, K.M., Harford-Wright, E., Vink, R., and Ghabriel, M.N. (2013). Characterisation of Walker 256 breast carcinoma cells from two tumour cell banks as assessed using two models of secondary brain tumours. Cancer Cell Int. *13*, 5.

36. Xu, L., Feng, Q., Deng, H., Zhang, X., Ni, H., and Yao, M. (2020). Neurexin-2 is a potential regulator of inflammatory pain in the spinal dorsal horn of rats. J. Cell Mol. Med. *24*, 13623–13633.

37. Lin, P.Y., Chen, L.Y., Jiang, M., Trotter, J.H., Seigneur, E., and Südhof, T.C. (2023). Neurexin-2, An inhibitory neurexin that restricts excitatory synapse formation in the hippocampus. Sci. Adv. *9*, eadd8856.

38. Chih, B., Engelman, H., and Scheiffele, P. (2005). Control of excitatory and inhibitory synapse formation by neuroligins. Science *307*, 1324–1328.

39. Gharami, K., and Biswas, S.C. (2020). Glutamate treatment mimics LTP- and LTD-like biochemical activity in viable synaptosome preparation. Neurochem. Int. *134*, 104655.

40. Kissiwaa, S.A., and Bagley, E.E. (2018). Central sensitization of the spino-parabrachial-amygdala pathway that outlasts a brief nociceptive stimulus. J. Physiol. *596*, 4457–4473.

41. Aroke, E.N., Joseph, P.V., Roy, A., Overstreet, D.S., Tollefsbol, T.O., Vance, D.E., and Goodin, B.R. (2019). Could epigenetics help explain racial disparities in chronic pain? J. Pain Res. *12*, 701–710.

42. Louwies, T., Ligon, C.O., Johnson, A.C., and Greenwood-Van Meerveld, B. (2019). Targeting epigenetic mechanisms for chronic visceral pain, A valid approach for the development of novel therapeutics. Neuro Gastroenterol. Motil. *31*, e13500.

43. Miller, C.P., Singh, M.M., Rivera-Del Valle, N., Manton, C.A., and Chandra, J. (2011). Therapeutic strategies to enhance the anticancer efficacy of histone deacetylase inhibitors. J. Biomed. Biotechnol. *2011*, 514261.

44. Zhou, H., Rauch, S., Dai, Q., Cui, X., Zhang, Z., Nachtergaele, S., Sepich, C., He, C., and Dickinson, B.C. (2019). Evolution of a reverse transcriptase to map N(1)-methyladenosine in human messenger RNA. Nat. Methods *16*, 1281–1288.

45. Nie, F., Tang, Q., Liu, Y., Qin, H., Liu, S., Wu, M., Feng, P., and Chen, W. (2022). RNAME, A comprehensive database of RNA modification enzymes. Comput. Struct. Biotechnol. J. *20*, 6244–6249.

46. Hong, S., Zheng, G., and Wiley, J.W. (2015). Epigenetic regulation of genes that modulate chronic stress-induced visceral pain in the peripheral nervous system. Gastroenterology *148*, 148–157.e7.

47. Sun, C., An, Q., Li, R., Chen, S., Gu, X., An, S., and Wang, Z. (2021). Calcitonin gene-related peptide induces the histone H3 lysine 9 acetylation in astrocytes associated with neuroinflammation in rats with neuropathic pain. CNS Neurosci. Ther. *27*, 1409–1424.

48. Xu, C., Zhao, B., Xu, L., Wang, Y., Liu, B., Xu, M., He, Q., Ni, C., Fu, J., Kong, M., et al. (2022). CXCR1 participates in bone cancer pain induced by Walker 256 breast cancer cells in female rats. Mol. Pain *18*. 17448069221135743.

49. Fu, J., Zhao, B., Ni, C., Ni, H., Xu, L., He, Q., Xu, M., Xu, C., Luo, G., Zhu, J., et al. (2021). Rosiglitazone Alleviates Mechanical Allodynia of Rats with Bone Cancer Pain through the Activation of PPAR-gamma to Inhibit the NF-kappaB/NLRP3 Inflammatory Axis in Spinal Cord Neurons. PPAR Res. *2021*, 6086265.

50. Fu, J., Ni, C., Ni, H.D., Xu, L.S., He, Q.L., Pan, H., Huang, D.D., Sun, Y.B., Luo, G., Liu, M.J., and Yao, M. (2021). Spinal Nrf2 translocation may inhibit neuronal NF-kappaB activation and alleviate allodynia in a rat model of bone cancer pain. J. Neurochem. *158*, 1110–1130.